A comparison of entrainment in turbulent line plumes adjacent to and distant from a vertical wall

Journal:	*Journal of Fluid Mechanics*
Manuscript ID	JFM-18-S-1604
mss type:	JFM Papers
Date Submitted by the Author:	20-Nov-2018
Complete List of Authors:	Parker, David; The University of Cambridge, DAMTP Burridge, Henry; Imperial College London, Civil and Environmental Engineering Partridge, Jamie; Centre for Mathematical Sciences, Department of Applied Mathematics and Theoretical Physics Linden, Paul; University of Cambridge, Department of Applied Mathematics and Theoretical Physics;
Keyword:	Plumes/thermals < Convection, Jets < Wakes/Jets, Turbulent convection < Turbulent Flows

Under consideration for publication in J. Fluid Mech.

A comparison of entrainment in turbulent line plumes adjacent to and distant from a vertical wall

D. A. Parker[1]†, H. C. Burridge[2], J. L. Partridge[1] AND P. F. Linden[1]

[1]Department of Applied Mathematics and Theoretical Physics, University of Cambridge, Centre for Mathematical Sciences, Wilberforce Road, Cambridge CB3 0WA, UK.
[2]Department of Civil and Environmental Engineering, Skempton Building, Imperial College London, London SW7 2AZ, UK.

(Received ?; revised ?; accepted ?. - To be entered by editorial office)

We present simultaneous two-dimensional velocity and buoyancy field measurements on a central vertical plane in two-dimensional line plumes: a free plume distant from all vertical boundaries and a wall plume, adjacent to a vertical wall. Data are presented in both an Eulerian frame of reference and a plume coordinate system that follows the instantaneous turbulent/non-turbulent interface (TNTI) of the plume. We present velocity and buoyancy measurements in both coordinate systems and compare the entrainment in the two flows and find that the value of the entrainment constant in the free plume is slightly less than double that of the wall plume. We show that this difference results from the wall plume physically entraining less than the free plume, for a given buoyancy flux. This reduction in entrainment resulting from the presence of the wall is investigated by considering the wall shear stress, the statistics of the TNTI and the conditional vertical transport of the ambient and engulfed fluid in both flows. We show that the wall shear stress in the wall plume is non-negligible and that the wall also inhibits the lateral meandering of the plume, compared to that observed for the free plume. The effect of the plume meandering on the entrainment process is quantified in terms of the stretching of the TNTI where it is shown that the total length of the TNTI in the free plume is greater than the wall plume by a factor of 2.5, and the relative vertical transport of the engulfed ambient fluid in the free plume is observed to be greater than in the wall plume by 15%. Finally, the turbulent velocity and buoyancy fluctuations and the turbulent velocity and buoyancy fluxes are presented for both flows in both an Eulerian and plume coordinate system. The conditional statistics show that the Reynolds stresses near the TNTI are larger in the wall plume consistent with a larger momentum jump at the edge of the wall plume. We also find that, at the viscous scale of the TNTI, the local entrainment velocity is on average greater in the wall plume than the free plume.

Key words:

---

1. Introduction

Buoyancy-driven wall bounded flows occur in both natural environments and industrial situations. The presence of a vertical wall in such flows is known to inhibit the process of turbulent entrainment (Lee & Emmons 1961) and thereby affect the mixing that arises.

† Email address for correspondence: dap58@cam.ac.uk

Here we investigate the effects of introducing a vertical wall to the flow generated by a line source of buoyancy. Applicable flows within effectively unbounded environments include the descending 'free' plume resulting from a chilled ceiling beam in the middle of a room, wherein the mixing of the plume affects the resulting thermal conditions within the room. In this paper we investigate the entrainment mechanisms and determine the extent to which the mixing of such plumes is altered if a chilled ceiling beam was placed adjacent to a wall, thereby producing a 'wall plume'.

A broad finding among the early studies of wall plumes (Lee & Emmons 1961; Ellison & Turner 1959; Turner 1973) is that the entrainment rates are significantly lower than those found in free plumes. Although velocity or buoyancy profile measurements were not presented in these studies, it was suggested that the wall suppresses the formation of large-scale structures and inhibits mixing, resulting in reduced entrainment into the plume. Velocity and buoyancy profiles are presented in later studies by Grella & Faeth (1975) and Lai & Faeth (1987), but in regions relatively close to the source where the flow was not self-similar. The only experimental velocity and buoyancy measurements of a wall plume in a self-similar region are those of Sangras *et al.* (1998) and Sangras *et al.* (2000), but they are not simultaneous. Nevertheless, the early findings of a reduced entrainment coefficient were confirmed, and entrainment approximately half that of a free plume was observed (Sangras *et al.* 1998). This reduction in entrainment was largely attributed to the reduced meandering of the large-scale structures and suppression of cross-stream turbulent fluxes (Ellison & Turner 1959; Turner 1973; Sangras *et al.* 2000).

Despite these insights, to our knowledge, a study examining and comparing the large-scale structures and cross-stream turbulent fluxes of a wall plume to those of a free plume does not exist. Burridge *et al.* (2017) examined an axisymmetric plume and suggested that engulfment of ambient fluid by the large scale structures is the rate-limiting process for turbulent entrainment. We follow a similar approach and seek to account for a reduced entrainment by examining the large-scale structures. This is achieved by making simultaneous measurements of velocity and buoyancy in self-similar line plumes adjacent to and far from a vertical wall. We also investigate the flow on small scales at the TNTI in order to elucidate their role in entrainment.

The paper is organised as follows. We review plume theory for two-dimensional free and wall plumes and the results of previous studies in § 2. The experimental methods and data analysis are presented in § 3, and the validation of the data is described in § 4. The experimental results in an Eulerian coordinate system are presented and discussed in § 5 and the same results are presented and discussed in a plume coordinate system in § 6. Finally, the conclusions are presented in § 7.

2. Theory and previous work on entrainment in free and wall plumes

A turbulent line plume is the flow driven by an infinitely long horizontal line source of buoyancy. The wall plume differs from the free plume by the presence of a vertical wall that is placed immediately adjacent to, and spans the entire length of, the line source. We consider a uniform ambient fluid and restrict attention to the case where the wall is adiabatic so that there is no loss or addition of buoyancy into the plume. Consequently, the buoyancy flux is constant with height in both the free plume and the wall plume. Here we outline the theory of entrainment in free and wall plumes in a quiescent environment. For a more comprehensive theory of entrainment the reader is referred to Paillat & Kaminski (2014) for free plumes and Grella & Faeth (1975) for wall plumes.

In both flows we define the vertical velocity $w(x, z, t)$ in the vertical z-direction, horizontal velocity $u(x, z, t)$ in the across-plume x-direction and the buoyancy $b(x, z, t) =$

$g(\rho_a - \rho)/\rho$, where ρ and ρ_a are the density of the plume and ambient, respectively. Since the flows are statistically steady, these quantities may be decomposed into time-averaged and fluctuating components $w(x,z,t) = \overline{w}(x,z) + w'(x,z,t)$, $u(x,z,t) = \overline{u}(x,z) + u'(x,z,t)$ and $b(x,z,t) = \overline{b}(x,z) + b'(x,z,t)$, and we denote the time-averaged maximum vertical velocity and buoyancy as $\overline{w}_m(z)$ and $\overline{b}_m(z)$. We assume all quantities are independent of the direction y aligned along the plume source. We define the time-averaged volume flux, momentum flux, integral buoyancy and buoyancy flux per unit length by

$$Q_f(z) = \int_{-\infty}^{\infty} \overline{w}(x,z)\mathrm{d}x, \qquad Q_w(z) = \int_{0}^{\infty} \overline{w}(x,z)\mathrm{d}x, \tag{2.1}$$

$$M_f(z) = \int_{-\infty}^{\infty} \overline{w}^2(x,z)\mathrm{d}x, \qquad M_w(z) = \int_{0}^{\infty} \overline{w}^2(x,z)\mathrm{d}x, \tag{2.2}$$

$$B_f(z) = \int_{-\infty}^{\infty} \overline{b}(x,z)\mathrm{d}x, \qquad B_w(z) = \int_{0}^{\infty} \overline{b}(x,z)\mathrm{d}x, \tag{2.3}$$

$$F_f(z) = \int_{-\infty}^{\infty} \overline{w}(x,z)\overline{b}(x,z)\mathrm{d}x, \qquad F_w(z) = \int_{0}^{\infty} \overline{w}(x,z)\overline{b}(x,z)\mathrm{d}x, \tag{2.4}$$

where the suffices f and w denote the free and wall plumes, respectively. From these relations we define the characteristic scales for plume half-width R and velocity W by

$$R_f = \frac{Q_f^2}{2M_f}, \qquad R_w = \frac{Q_w^2}{M_w}, \tag{2.5}$$

$$W_f = \frac{M_f}{Q_f}, \qquad W_w = \frac{M_w}{Q_w}. \tag{2.6}$$

Note that in the case of the wall plume the full width of the flow R_w is used since it is analogous to the half-width of the free plume.

For the free plume, under the entrainment assumption, the inflow velocity at any height is proportional to the local vertical plume velocity i.e. $u(-\infty, z) = -u(\infty, z) = \alpha_f W_f$, where α_f is the 'top-hat' entrainment constant (Morton *et al.* 1956), and the Boussinesq time-averaged volume, momentum and buoyancy flux conservation equations may be written as

$$\frac{\mathrm{d}Q_f}{\mathrm{d}z} = 2\alpha_f \frac{M_f}{Q_f}, \tag{2.7}$$

$$\frac{\mathrm{d}M_f}{\mathrm{d}z} = B_f = \frac{\theta_f F_f Q_f}{M_f}, \tag{2.8}$$

$$\frac{\mathrm{d}F_f}{\mathrm{d}z} = 0, \tag{2.9}$$

where θ_f encapsulates the relation between the integral buoyancy B_f and the buoyancy flux F_f, which by assuming self-similarity we may take as constant. Note that in (2.7) the factor of two occurs as α_f is the entrainment into one side of the plume only. The solutions to the free plume equations (2.7)-(2.9) are

$$Q_f(z) = (2\alpha_f)^{2/3} (\theta_f F_f)^{1/3} z, \tag{2.10}$$

$$M_f(z) = (2\alpha_f)^{1/3} (\theta_f F_f)^{2/3} z, \tag{2.11}$$

$$F_f(z) = F_f. \tag{2.12}$$

Under the same assumptions, in particular the equivalent entrainment assumption that $u(\infty, z) = -\alpha_w W_w$, the time-averaged volume, momentum and buoyancy conservation

flux equations for the wall plume may be written as

$$\frac{\mathrm{d}Q_w}{\mathrm{d}z} = \alpha_w \frac{M_w}{Q_w}, \tag{2.13}$$

$$\frac{\mathrm{d}M_w}{\mathrm{d}z} = B_w - \epsilon = \frac{\theta_w F_w Q_w}{M_w} - C\left(\frac{M_w}{Q_w}\right)^2, \tag{2.14}$$

$$\frac{\mathrm{d}F_w}{\mathrm{d}z} = 0, \tag{2.15}$$

where θ_w encapsulates the relation between the integral buoyancy B_w and the buoyancy flux F_w, and ϵ is the wall shear stress, which we express in terms of the characteristic velocity W_w and a (constant) skin friction coefficient C. The assumption of self-similarity in the wall plume is more problematic because of the existence of a viscous boundary layer in order to satisfy the no-slip condition on the vertical wall. However, throughout this paper we assume the wall plume is self similar, which is justified in § 4. Therefore, we take θ_w and C to be constants. Then the solutions to the wall plume equations (2.13)-(2.15) are

$$Q_w(z) = \left(\frac{\theta_w F_w}{1+\frac{C}{\alpha_w}}\right)^{1/3} \alpha_w^{2/3} z, \tag{2.16}$$

$$M_w(z) = \left(\frac{\theta_w F_w}{1+\frac{C}{\alpha_w}}\right)^{2/3} \alpha_w^{1/3} z, \tag{2.17}$$

$$F_w(z) = F_w. \tag{2.18}$$

The constants α_w and α_f are the standard top-hat entrainment coefficients. However, it has been widely observed in previous studies that the vertical velocity and buoyancy profiles of a free plume are well fitted by a Gaussian, and the conservation of volume flux in the free and wall plume may also be expressed in terms of the maximum vertical velocity and a Gaussian entrainment coefficient α_G, in the form

$$\frac{\mathrm{d}Q_f}{\mathrm{d}z} = 2\alpha_{f,G}\overline{w}_m, \quad \frac{\mathrm{d}Q_w}{\mathrm{d}z} = \alpha_{w,G}\overline{w}_m. \tag{2.19}$$

The top-hat entrainment coefficient in the free plume is related to the Gaussian coefficient by $\alpha_f = \sqrt{2}\,\alpha_{f,G}$ and most studies choose to calculate $\alpha_{f,G}$. At present there is significant disagreement about the value of the entrainment coefficient, with previously reported equivalent top-hat values in the range $\alpha_f = \{0.13, 0.20\}$ (table 1).

Most studies on wall plumes also focus on the Gaussian entrainment constant $\alpha_{w,G}$, although in some cases, notably Grella & Faeth (1975), the top hat value α_w was also calculated. Since the velocity profile of the wall plume is not a known analytic function a theoretical relation between α_w and $\alpha_{w,G}$ has not been derived, although Grella & Faeth (1975) find that $\alpha_w/\alpha_{w,G} \approx 1.4$. There is broad agreement with previously measured Gaussian entrainment values of the wall plume (table 1). The agreement of the Gaussian entrainment values is somewhat surprising given the additional difficulties associated with measuring the velocity of the wall-plume, which is perhaps reflected in the variation in other parameters between these experiments, especially the maximum mean velocity used in the calculation of $\alpha_{w,G}$. Further, Grella & Faeth (1975) and Lai & Faeth (1987) emphasise that their data were not in a self-similar region as the flow appeared to be evolving over the whole range of heights where the measurements were taken. For these reasons it appears that, to our knowledge, an experimentally determined

Experiment	α	α_G	$\overline{w}_m/F_o^{1/3}$	$\frac{\mathrm{d}Q}{\mathrm{d}z}/F_o^{1/3}$	Plume type
Lee & Emmons (1961)	-	0.16	-	-	Free
Kotsovinos (1975)	-	0.10	1.66	-	Free
Yuana & Cox (1996)	-	0.13	2.04	-	Free
Paillat & Kaminski (2014)	-	0.12	$2.1 - 2.2$	-	Free
Ramaprian & Chandrasekhara (1989)	0.16	0.11	2.13	0.46	Free
Rouse *et al.* (1952)	-	0.11	1.91	-	Free
Present study	0.14	0.10	2.12	0.40	Free
Grella & Faeth (1975)	0.095	0.067	3.16	0.21	Wall
Lai & Faeth (1987)	-	0.071	2.14	0.15	Wall
Sangras *et al.* (2000)	-	0.068	2.84	0.19	Wall
Present study	0.08	0.061	2.73	0.17	Wall

TABLE 1. Entrainment values, scaled vertical velocities and scaled rate of change of mean volume flux of previous work, where F_o is the source buoyancy flux.

Experiment	$Q_0\,[\times 10^{-4}\,\mathrm{m^2\,s^{-1}}]$	$b_0\,[\mathrm{m\,s^{-2}}]$	Γ	Re	$\eta[\times 10^{-4}\,\mathrm{m}]$	$\lambda_B[\times 10^{-6}\,\mathrm{m}]$	PIV scale	LIF scale
Free								
1	1.33	0.24	1.10	1860	1.1	4.9	10η	$19\lambda_B$
2	1.33	0.24	0.99	1900	1.1	4.9	10η	$19\lambda_B$
3	1.00	0.24	1.16	1660	1.2	5.9	9η	$16\lambda_B$
4	1.22	0.21	0.91	1440	1.1	4.8	10η	$19\lambda_B$
5	1.22	0.21	0.98	1620	1.1	4.8	10η	$19\lambda_B$
Wall								
6	0.79	0.33	1.55	2600	1.0	4.5	11η	$20\lambda_B$
7	0.79	0.33	1.87	2420	1.0	4.5	11η	$20\lambda_B$
8	1.03	0.33	1.95	2800	0.9	4.1	12η	$21\lambda_B$
9	1.02	0.16	1.97	2950	0.9	4.1	12η	$21\lambda_B$
10	1.02	0.16	1.75	2610	1.0	4.6	11η	$19\lambda_B$

TABLE 2. Experimental parameters of the plume experiments.

top-hat entrainment value for a wall-plume within a self-similar region does not exist in the literature. This is problematic given the unknown relationship between $\alpha_{w,G}$ and α_w in a self-similar region, and despite the consistency between the previously determined $\alpha_{w,G}$ the closure model of (2.19) relies on an established maximum velocity for which there is significant disagreement.

Our study is focused on the comparison of the top-hat entrainment values for a free and a wall plume. Since these two flows have different velocity profiles it is natural to compare the entrainment rates without any assumption on profile shapes. It is, therefore, unfortunate that for the wall plume case previous work has paid less attention to the top-hat value.

3. Experiments and analysis

3.1. *Experimental details*

The experiments were designed to create turbulent free and wall plumes that would enable us to make simultaneous measurements of the buoyancy and velocity fields of the flow. The experiments were performed in a Perspex (acrylic) tank of horizontal cross-section $1.2\,\mathrm{m} \times 0.4\,\mathrm{m}$ filled with dilute saline solution of uniform density ρ_a to a depth of $0.75\,\mathrm{m}$. Relatively dense sodium nitrate solution was used as source fluid which enabled refractive indices of the plume fluid and ambient to be matched as is needed for accurate measurements of the velocity field as described below. The source fluid, at a relative

density of b_0, was supplied by a gear pump which provided a uniform volume flux Q_0 and buoyancy flux $F_0 = Q_0 b_0$ per unit length, via a line source of dimension $l = 0.15\,\mathrm{m}$ and width $d = 1\,\mathrm{mm}$. The flow was enclosed by two $0.6\,\mathrm{m} \times 0.6\,\mathrm{m}$ transparent walls (x-z planes) perpendicular to the line source, separated by the length of the source, to promote the two dimensionality of the flow by eliminating any entrainment from beyond the ends of the source. To create the wall plume a further vertical wall in the y-z plane was mounted immediately adjacent to one edge of the line source. The fluid was seeded with particles of mean diameter 20 µm in order to perform particle image velocimetry (PIV). Videos were recorded and processed at a frame rate of 100 Hz. The PIV was processed at a spatial resolution of 1.06 mm. The buoyancy field was measured simultaneously, via a separate camera, using laser induced fluorescence (LIF). This was accomplished by adding a small amount of Rhodamine 6G to the source solution. At the concentrations used the light intensity exhibits a linear relationship with the dye concentration, so that the buoyancy, which is proportional to plume fluid concentration, may be determined. The spatial resolution of the processed LIF images was 0.088 mm, a factor of 12 smaller than the resolution of the PIV.

In both cases it is necessary to eliminate refractive index variations within the fluid as these produce distortions of the light paths and lead to errors in determining the positions of the PIV particles and uncertainty in the location of the dye measurements. As mentioned above the use of sodium nitrate solutions for the plume and sodium chloride solution for the ambient fluid allows density differences while keeping the same refractive index. The refractive indices were matched to within 0.05%.

To allow simultaneous measurements of velocity and density, a 532 nm laser was used to create a light sheet 2 mm thick, and a narrow bandpass filter (centred at the wavelength of the laser) was placed before the PIV cameras so only the scattered light from the PIV particles was detected. Rhodamine 6G emits light at a peak wavelength of 552 nm when excited by a laser at 532 nm, so to isolate the density field a longpass filter was placed before the LIF camera so that only the fluoresced signal from the Rhodamine 6G was captured.

Measurements for the free plume were collected 0.17 m from the physical source over a distance of 0.15 m and measurements for the wall plume were collected 0.32 m from the physical source over a distance of 0.15 m. These regions were sufficiently far from the source so that the plumes can be considered pure and self-similar. We verified that the plumes satisfy the pure-plume criterion used by Paillat & Kaminski (2014) of an invariant maximum velocity with height. In addition, we checked that the Richardson number was invariant with height. A total of 10 plumes were studied, 5 free plumes and 5 wall plumes, and the experimental source parameters are given in table 3.1. Also given are the Reynolds number $\mathrm{Re} = \overline{w}_m R/\nu$ at the mid-height of the region examined, where R is the plume half-width defined in (2.5) and the plume parameter Γ, averaged over the total height of the region examined, where

$$\Gamma_f = \frac{Q_f^3 F_f}{2\alpha_f M_f^3}, \qquad \Gamma_w = \frac{Q_w^3 F_w}{\alpha_w M_w^3}. \tag{3.1}$$

We calculate the Kolmogorov length scale, $\eta = R/\mathrm{Re}^{3/4}$, and the Batchelor scale, $\lambda_B = \eta/Sc^{1/2}$. Table 3.1 shows that the resolution of the LIF images was much greater than the Batchelor scale, suggesting that the effects of diffusion at these scales may be ignored in our analysis.

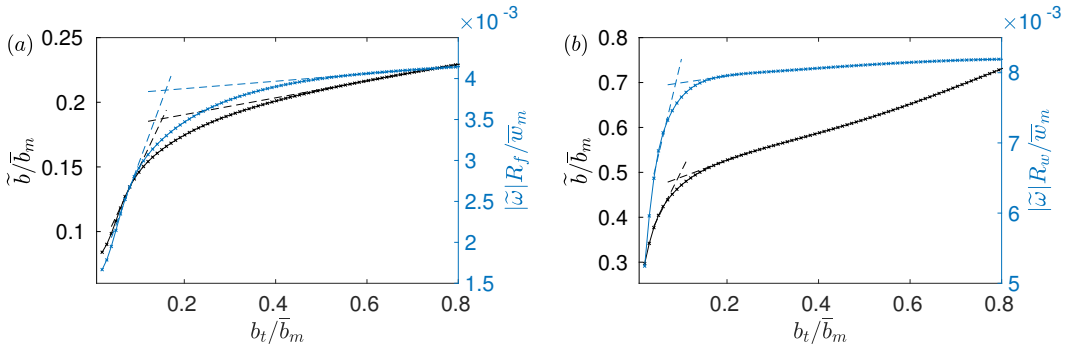

FIGURE 1. Identification of the scalar threshold b_t used to identify the TNTI of the (a) free and (b) wall plume. A sharp change in the gradient of the conditional mean buoyancy (black) and conditional vorticity magnitude (blue) was found to coincide in both cases at a value of $b_t = 0.16$ and $b_t = 0.09$ for the free and wall plume, respectively.

3.1.1. *Detection of the TNTI*

The TNTI of the plume and conditional statistics, based on the presence or absence of plume fluid which are separated by the TNTI, were used to characterise the flow. Therefore, it was crucial that we were able to accurately detect and distinguish between ambient fluid and plume fluid. Given that the Batchelor scale of the plumes was small compared to the resolution of the LIF measurements, we were able to employ a similar method to that used by Prasad & Sreenivasan (1989) and Mistry *et al.* (2016) to find the TNTI in an axisymmetric jet. This involved identifying the TNTI by a scalar threshold b_t, which coincides with a rapid change in the gradient of the conditional mean buoyancy $\widetilde{b}$ and spanwise vorticity magnitude $|\widetilde{\omega_y}|$, where the conditional mean is defined by

$$\widetilde{f(b_t)} = \frac{\int\int (f(x,z)\mathrm{d}x\mathrm{d}z)\,|_{b>b_t}}{\int\int \mathrm{d}x\mathrm{d}z|_{b>b_t}}. \tag{3.2}$$

Mistry *et al.* (2016) also consider the conditional mean vertical velocity in their identification of b_t, however, given the findings of Burridge *et al.* (2017) that significant vertical velocities exist outside the scalar edge of an axisymmetric plume, we chose to consider instead only the buoyancy and spanwise vorticity, as the flow outside the plume is irrotational. The TNTI locations, based on both the buoyancy and the vorticity, were found to coincide with threshold values $b_t/\overline{b}_m = 0.16$ and $b_t/\overline{b}_m = 0.09$ for the free and wall plume, respectively (figure 1). The observation that the threshold of the wall plume is approximately half that of the free plume results from the fact that it is scaled by the maximum time-averaged buoyancy, which is approximately double in the wall plume for a given buoyancy flux and distance from the source, as will be verified in § 4. We may now consider regions $b < b_t$ to be ambient fluid and regions $b > b_t$ to be plume fluid.

4. Validation of the PIV and LIF data

We first validate the plume data by demonstrating the self-similar behaviour of the velocity and buoyancy profiles. Figures 2 and 3 show the vertical and horizontal velocities and buoyancy profiles for ten different heights from each experiment, where the x-axis is scaled on the virtual distance from the source, $z - z_0$, where z_0 is the virtual origin. The virtual origin was calculated by identifying, by linear extrapolation, the vertical location at which the plume width is zero. A good collapse of data on to a single curve is seen in

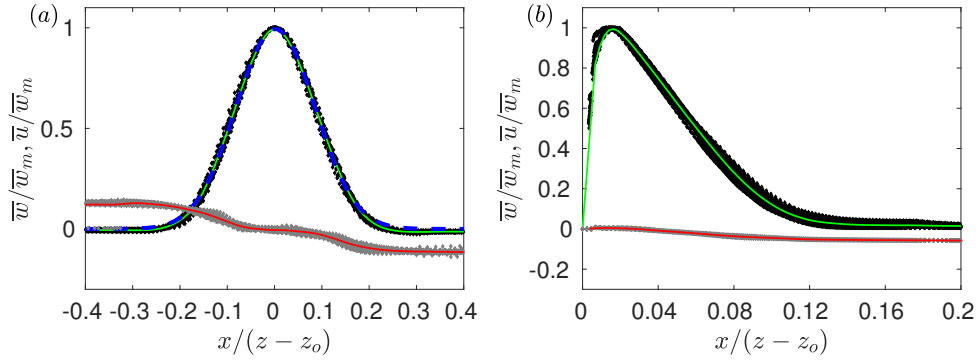

FIGURE 2. Time-averaged scaled vertical, black, and horizontal, grey, velocity profiles of the (*a*) free and (*b*) wall plume. For each experiment, ten different heights spanning the studied region are plotted. The average values of all the data for the vertical, green, and horizontal, red, velocities are shown in each case. The best-fit curve for the vertical velocity of the free plume has been fitted using a Gaussian least-squares fit, shown in blue.

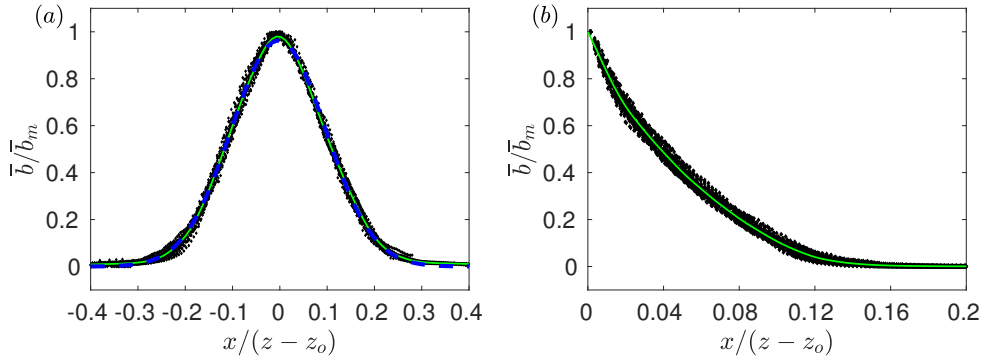

FIGURE 3. Time-averaged scaled buoyancy profiles of the (*a*) free and (*b*) wall plume. For each experiment, ten different heights spanning the studied region are plotted. The average values of all the data for the buoyancy are shown in green and the best-fit curve for the buoyancy of the free plume has been fitted using a Gaussian least-squares fit, shown in blue.

each plot. The self-similar vertical velocity and buoyancy profiles of the free plume are fitted well by a Gaussian curve (shown by the dashed blue curve) as has been previously observed (e.g Paillat & Kaminski (2014), Ramaprian & Chandrasekhara (1989)) and the wall plume profiles agree well with those of Sangras *et al.* (1999) and Sangras *et al.* (2000). Further confidence in the self-similarity of the plumes is given by the invariance with height of the maximum vertical velocity, scaled by the buoyancy flux $F_0^{1/3}$, shown in figure 4, and the inverse linear decay $\sim 1/z$ (Fischer *et al.* 1979) of the top-hat buoyancy B/R shown in the compensated plot in figure 5.

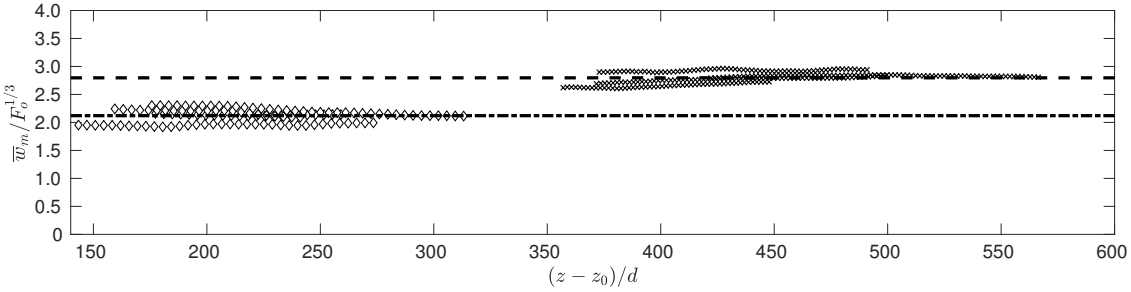

FIGURE 4. Maximum vertical velocities of the free (diamonds) and wall plume (crosses), scaled using the source buoyancy flux. The mean values across all experiments are shown by the horizontal dashed lines.

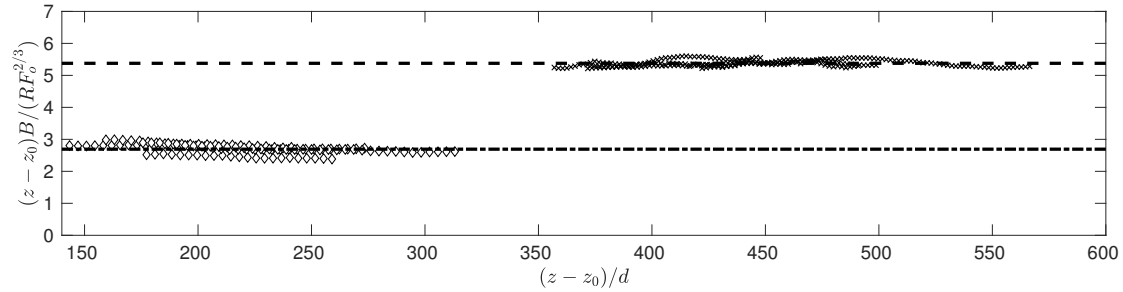

FIGURE 5. Time-averaged top hat buoyancy of the free (diamonds) and wall plume (crosses), scaled using the vertical distance and source buoyancy flux. The mean values across all experiments are shown by the horizontal dashed lines.

5. Results in an Eulerian coordinate system

5.1. *Entrainment coefficient*

The top-hat entrainment coefficients for the free and wall plume were determined from the solutions of the conservation equations (2.10)-(2.12) and (2.16)-(2.18), respectively. A least squares best-fit to the plume half-width R (figure 6) gives

$$\alpha_f = \frac{\mathrm{d}R_f}{\mathrm{d}z} = 0.14 \pm 0.01, \quad \alpha_w = \frac{\mathrm{d}R_w}{\mathrm{d}z} = 0.08 \pm 0.008, \tag{5.1}$$

where the tolerances indicate the standard deviation in the values measured across the five independent experiments examined in each case. Our value of α_f lies within the range, but near the lower end, of previously reported entrainment coefficients, $\alpha_f = \{0.13, 0.20\}$. Our value of α_w is lower than the previously reported value of $\alpha_w = 0.095 \pm 0.005$ in Grella & Faeth (1975). In particular, our results support previous studies that find α_w is slightly more than half of α_f. We note that, for the time-averaged flows, if we were to consider the wall plume as 'half' the free plume, we would expect the top-hat entrainment values to be equal to one another since the equation expressing conservation of volume flux in the free plume (2.7) accounts for the double-sided entrainment with the factor of 2. Consequently, this difference is a result of the absence or presence of the wall.

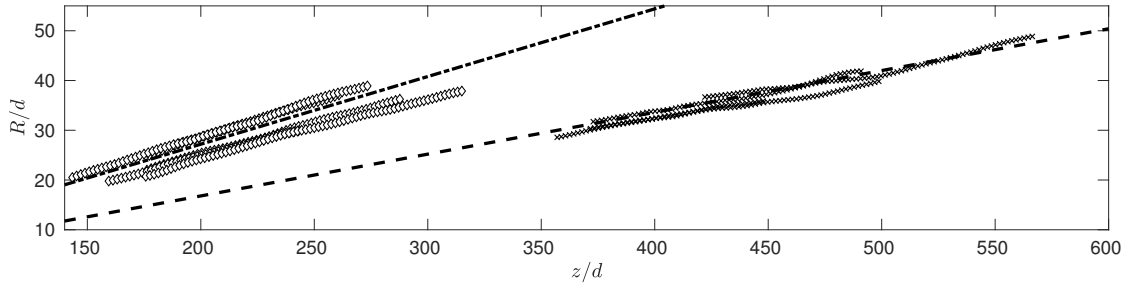

FIGURE 6. The variation in the mean plume half-width, R/d (2.5), for the free plume (diamonds) and wall plume (crosses). A line of best fit, used to calculate the entrainment values (5.1), are shown by the respective dashed lines.

The entrainment coefficient may be viewed as a measure of the plume entrainment efficiency. However, to interpret the physical implications we consider how much fluid is entrained into the free and wall plume per unit height. For a given buoyancy flux $F = F_w = F_f$, (2.10) and (2.16) give

$$\frac{2u_{\infty,f}}{u_{\infty,w}} = \frac{\mathrm{d}Q_f}{\mathrm{d}z}\left(\frac{\mathrm{d}Q_w}{\mathrm{d}z}\right)^{-1} = 2^{2/3}\left(\frac{\alpha_f}{\alpha_w}\right)^{2/3}\left(1+\frac{C}{\alpha_w}\right)^{1/3}, \tag{5.2}$$

where we have used that $(\theta_f/\theta_w)^{1/3} \approx 1$, as verified from our data.

The coefficient of friction C was found from balancing the momentum equation (2.14), and a best-fit to our data gives $C = 0.015 \pm 0.005$. We note the difficulties in this approach, due to the the omission of the vertical velocity fluctuations and pressure term, the latter of which can not be measured directly, in the vertical momentum equation, which together have been shown to account for up to 8% of the mean vertical momentum in an axisymmetric plume (van Reeuwijk *et al.* 2016). Therefore, we do not place emphasis on our result of the skin friction coefficient, and note that our conclusions are qualitatively the same for any (reasonable) values of $C \geq 0$. Using the entrainment values (5.1) in the right hand side of (5.2) we find that $2u_{\infty,f}/u_{\infty,w} = 2.45 \pm 0.35$. This agrees with direct measurements of $(\mathrm{d}Q_f/\mathrm{d}z)/(\mathrm{d}Q_w/\mathrm{d}z) = 2.35 \pm 0.1$. Hence, despite the value of the entrainment coefficient for a free plume being less than double that of the wall plume, the increase in volume flux with height in a free plume is significantly greater than double that of a wall plume with equal forcing i.e. equivalent buoyancy flux. This implies that each edge of the free plume entrains ambient fluid more efficiently than the wall plume, per unit height.

5.2. *The statistics of the TNTI*

Figure 7 shows an instantaneous image taken from our experiments of both the free and wall plume. The continuous outer TNTI has been identified and highlighted in white. Also highlighted, in red, are the TNTIs of regions of unmixed ambient fluid completely engulfed, within the plane, by plume fluid. In both flows, there are significant deviations from the positions of the mean outer TNTI, denoted by the dashed magenta lines. The meandering nature of the free plume is evident from figure 7(a), where in addition to the relatively small coherent structures forming, i.e eddies along the outer TNTI, which are

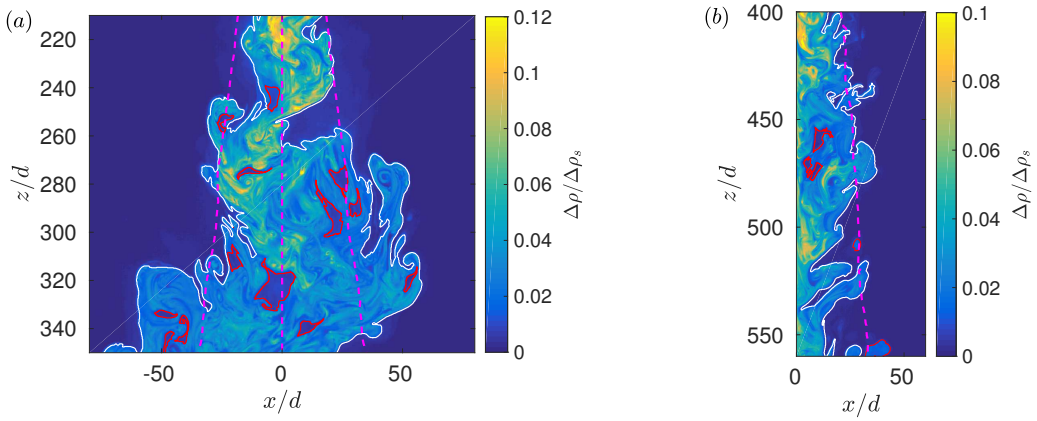

FIGURE 7. Instantaneous buoyancy field of the (a) free and (b) wall plume. The figures shown are the processed LIF images at full resolution, which corresponds to an effective filter size of (a) $\Delta/\eta_h = 0.8$ and (b) $\Delta/\eta_h = 0.9$. In both cases the outer continuous TNTI is highlighted by the solid white line and the TNTIs of unconnected regions and completely engulfed ambient fluid are highlighted by the red lines. The TNTIs were identified from the threshold b_t determined in § 3.1.1. In (a) the mean position of the outer left TNTI, centreline and outer right TNTI are denoted by the dashed magenta lines from left to right. In (b) the position of the mean outer TNTI of the free plume is denoted by the dashed magenta line.

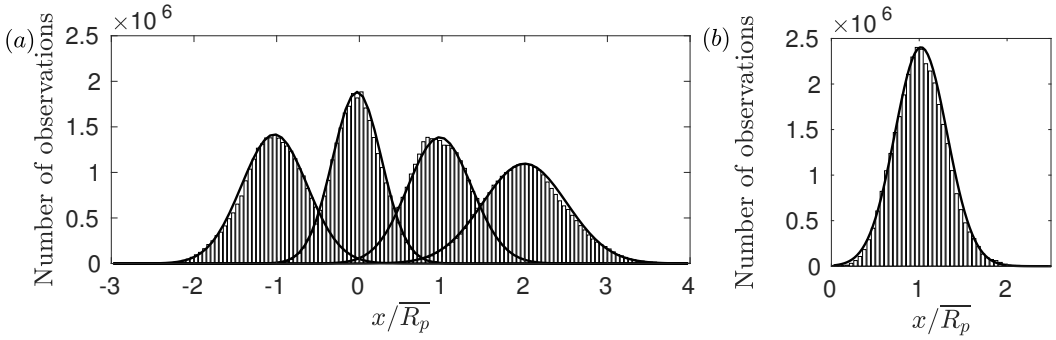

FIGURE 8. Histograms of (a) the locations (from left to right) of the left-TNTI, the centre, the right-TNTI and the plume scalar width of the free plume and (b) the plume scalar half-width of the wall plume. All distances have been normalised by the time-average plume scalar half-width, $\overline{R_p}$. The solid curves are Gaussian best fits to the data.

also seen in the wall plume, the free plume also forms coherent structures at the length scale of the full plume width. As a result the instantaneous edge of the wall plume is comparatively closer to the mean TNTI (figure 7(b)) than for the free plume.

Histograms of the outer left, E_L, and right, E_R, TNTI of the free plume and outer edge of the wall plume, R_p, are shown in figure 8, normalised by the time-averaged scalar half-width of the plume. We define the instantaneous plume scalar half-width and centreline as, $R_p = (E_R - E_L)/2$, and, $C = (E_R + E_L)/2$, respectively for the free plume and the scalar half-width as the distance from the wall to the outer TNTI in the wall plume. We find that the positions of the left and right TNTI of the wall

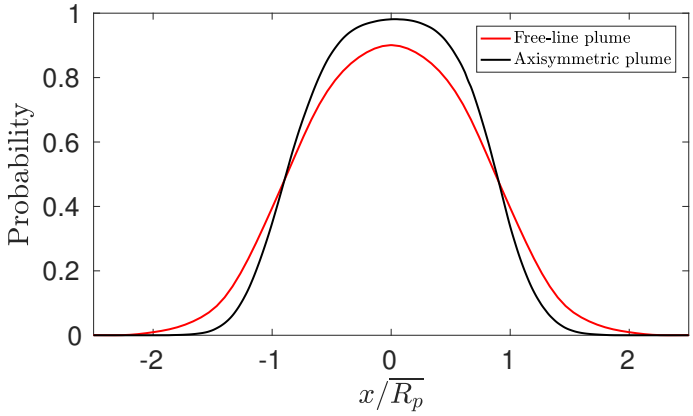

FIGURE 9. The probability, at a given horizontal location, of being within the plume region bounded by the outer TNTI for the free plume, red, and for comparison an axisymmetric plume, black (Burridge *et al.* 2017).

plume are both well represented by Gaussian distributions $E_L \sim N(\mu = -1, \sigma^2 = 0.16)$, $E_R \sim N(\mu = 1, \sigma^2 = 0.16)$, respectively, where μ denotes the mean and σ the standard deviation. The free plume scalar half-width and centreline are also approximated by Gaussian distributions, $2R_p \sim N(\mu = 2, \sigma^2 = 0.27)$, $C \sim N(\mu = 0, \sigma^2 = 0.093)$. For the wall plume, we find that $R_p \sim N(\mu = 1, \sigma^2 = 0.088)$. In the case of the free plume, since $C = (E_R + E_L)/2$, it follows that the Pearson's correlation coefficient, $\rho_{E_R,E_L} = 0.16$. This may compared to an axisymmetric plume where it was found that $\rho_{E_R,E_L} = 0$ (Burridge *et al.* 2017). So although the correlation between the two edges is larger than that for an axisymmetric plume, it is still small.

However, this statistic masks the true meandering nature of the plume as is evident from figure 7 (*a*). The position of the outer left and right TNTI of the free plume at, say, $z/d = 260$ line do not demonstrate meandering, even though the body of the plume has clearly meandered to the left and overturned. For this reason, the meandering nature of the plume is more robustly demonstrated by considering the probability, at given horizontal location, of plume fluid being within the connected region that is bounded by the outer plume TNTI, as shown in figure 9. This demonstrates that there is a significant probability $\sim 15\%$ that a connected region of ambient fluid exists at the mean centreline of the plume, as a result of the plume meandering. For comparison, the equivalent probability function for an axisymmetric plume, which does not demonstrate a meandering behaviour, is shown (Burridge *et al.* 2017), and the probability is much lower $\sim 1\%$. Kotsovinos (1975) and Westerweel *et al.* (2005) have performed similar statistics for a free line and axisymmetric jet, respectively, and also find that there is a finite but very low probability of ambient fluid existing at the mean centreline. We note that Kotsovinos (1975) also calculated the plume fluid intermittency for a free line plume, and found it was almost identical to that free jet, which appears to be inconsistent with his observations of plume meandering.

To quantify the effect of the meandering on the TNTI of the free plume we consider the length of the TNTI of the free and wall plume. We use a methodology similar to that of Mistry *et al.* (2018), where box filtering, of size Δ, is applied to each instantaneous image and the TNTI is identified from the scalar threshold b_t. Figure 7 shows the result

of this method for the minimum box filter used of $\Delta/\eta_h = 0.8$ and 0.9 for the free and wall plumes, respectively where η_h is the Kolmogorov length scale measured at the mid height of the data. Completely engulfed and unconnected regions are included in the calculation which are non-negligible in the flows we are considering.

The results for varying box sizes $0.8 < \Delta/\eta_h < 42$ (the resolution of our buoyancy field measurements was limited to approximately $0.8\eta_h$) are shown in figure 10. The mean interface length $\overline{L_s}$ is normalised by the projected interface length L_z, which is defined by the vertical distance of the region considered in the wall-plume and twice the vertical distance in the free plume. We find that the mean length of total the TNTI of the free plume is larger than that of the wall plume by a factor of about 2.5. Figure 10 (b) shows that this value varies by less than 1%, for measurements where $\Delta/\eta_h < 2$. Further, the magnitude of the gradient is monotonically decreasing for $\Delta/\eta_h < 8$ which suggests that $\overline{L_{s,f}}/\overline{L_{s,w}} \approx 2.5$ for $\Delta/\eta_h < 1$.

Note that it is expected that our results may vary depending on the size of the Kolmogorov length scale. In particular, for $\Delta = \eta$, we expect $\overline{L_s}/L_z = f(\eta)$, for some function f. However, since $\eta \sim z^{1/4}$ and over the height of our data η varied by at most 10%, we expect the value of f to be effectively constant. In addition, regions at varying distances from the source were tested, where at all heights $\Delta_{min} < \eta$, and no significant deviation from our results were found, so we are confident this result is robust.

The implications of this result for the small scale entrainment, local to the TNTI, may be considered by comparing the global entrainment flux with the total flux across the TNTI. Meneveau & Sreenivasan (1990) suggested that the total flux across the TNTI should be independent of scale. An equivalent relation for the entrainment velocity u_∞ is the following (Mistry *et al.* 2016),

$$u_\infty = \frac{1}{L_z}\overline{\int_0^{L_s(\Delta)} u_n(\Delta) ds}, \tag{5.3}$$

where $u_n(\Delta)$ is the entrainment velocity normal to the TNTI and the integral is performed over the path of the interface, $L_s(\Delta)$. The right hand side of (5.3) may be rewritten in terms of a mean local entrainment velocity $U_n(\Delta)$ and the mean length of the TNTI, so that $u_\infty = U_n(\Delta)\overline{L_s}(\Delta)/L_z$. By using the results of this section and § 5.1 we may compare the mean local entrainment velocity, at the viscous scale $\Delta \approx \eta$, of the free plume $U_{n,f}$ and wall plume $U_{n,w}$ for a given buoyancy flux,

$$\frac{U_{n,f}(\Delta \approx \eta)}{U_{n,w}(\Delta \approx \eta)} = \frac{u_{\infty,f}}{u_{\infty,w}} \frac{\overline{L_{s,w}}(\Delta \approx \eta)}{\overline{L_{s,f}}(\Delta \approx \eta)} = 0.94 \pm 0.05. \tag{5.4}$$

This states that the average local entrainment velocity at the viscous scale is greater in the wall plume. Further, since $\overline{L_s}(\Delta \approx \eta)/L_z \approx$ const. this suggests that $U_n(\Delta \approx \eta) \approx$ const. i.e independent of z over the height of our experiments.

5.2.1. *Scaling of the TNTI*

While the main purpose of calculating the mean length of the TNTI of the two flows was to compare the relative lengths, this type of analysis has also been used to consider the fractal scaling of the TNTI of boundary layers (de Silva *et al.* 2013) and jets (Mistry *et al.* 2016). We apply the same analysis to the free and wall plume.

Typically, one considers the number N of boxes of size Δ that are required to cover the TNTI. The fractal scaling is then given by $N \sim \Delta^{-D}$, for a fractal dimension D. de Silva *et al.* (2013) show that the box filtering method employed above may also be used to determine D given that one expects $\overline{L_s} \sim \Delta N \sim \Delta^{1-D}$. Figure 10 shows that

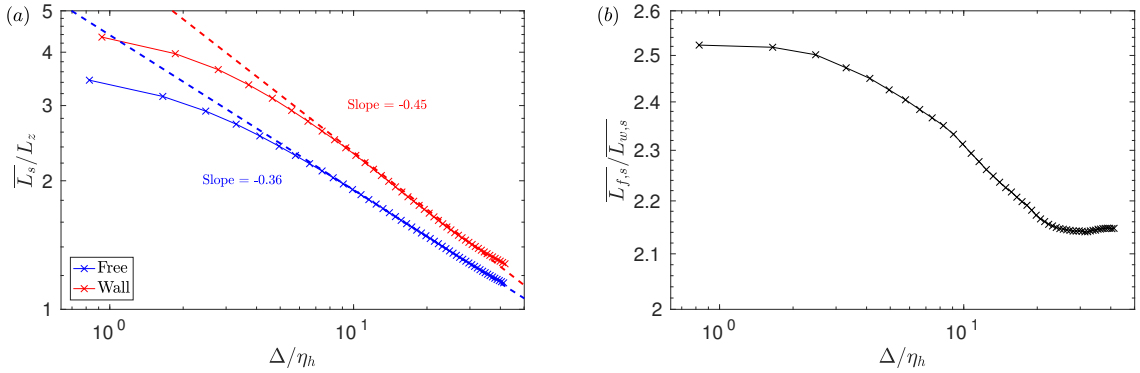

FIGURE 10. (*a*) Mean TNTI length for varying box filter sizes, $0.8 \leq \Delta/\eta_h \leq 42$ for the free plume, red, and wall plume, blue. The lengths have been scaled by the projected length of the interface. The slopes of the profiles over the inertial range have been overlaid with dashed lines. (*b*) The ratio of the mean TNTI length of the free plume, $\overline{L_s^f}$, and the wall plume, $\overline{L_s^w}$.

for the free plume $D_f = 1.45$, calculated from the best-fit of the slope of the profile over the range $7 \leq \Delta/\eta_h \leq 29$, and for the wall plume $D_w = 1.36$, calculated from the best-fit of the slope of the profile over the range $5 \leq \Delta/\eta_h \leq 35$. The tailing-off effect for small and large filter sizes in figure 10 (*a*) is also observed by Mistry *et al.* (2016) for axisymmetric jets and suggests these regions are outside the fractal scaling range. For a turbulent boundary layer de Silva *et al.* (2013) find a fractal dimension of $D = 1.3$ to 1.4, consistent with the value we find for the wall plume. However, we find a significantly larger value for the free plume, which has not been observed in other free-shear flows where, for example, Mistry *et al.* (2016) find that $D = 1.33$ for an axisymmetric jet.

5.3. *Conditional vertical transport*

In order to quantify the effect of the meandering of the free plume on the large scale engulfment we calculate the conditional vertical transport of ambient fluid, for both the free and wall plumes, by considering, separately, ambient fluid outside the TNTI envelope and engulfed but unmixed fluid. In order to calculate the fluxes of the ambient fluid we follow a method equivalent to that of Burridge *et al.* (2017) by first defining an instantaneous step function for the outer ambient fluid

$$H_{out} = \begin{cases} 0 \text{ for } E_L(z,t) < x < E_R(z,t), \\ 1 \text{ otherwise,} \end{cases} \tag{5.5}$$

and a step function for all unmixed fluid

$$H_{amb} = \begin{cases} 0 \text{ for } b(x,z,t) > b_t(z), \\ 1 \text{ for } b(x,z,t) < b_t(z). \end{cases} \tag{5.6}$$

A step function identifying the locations of engulfed but unmixed fluid H_{eng} is then given by $H_{eng} = H_{amb}[1 - H_{out}]$. The time-averaged volume flux of ambient fluid outside the plume TNTI envelope is then given by

$$\overline{Q_{out}}(z) = \frac{1}{T}\int_0^T \int H_{out}(x,z,t)w(x,z,t)\mathrm{d}x\mathrm{d}t, \tag{5.7}$$

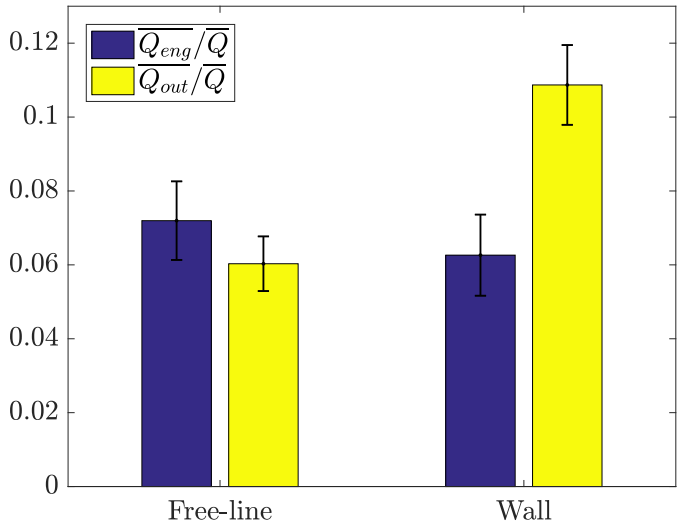

FIGURE 11. Time-averaged conditional volume flux of the ambient fluid outside the plume envelope (yellow) and of engulfed but unmixed ambient fluid (blue) for both the free and wall plume. The error bars denote the standard deviation amongst the five experiments considered.

where the integral domains over the x-coordinate are given by the respective domains of the free plume $(-\infty, \infty)$ and wall plume $(0, \infty)$. Similarly, the time-averaged volume flux of engulfed but unmixed fluid is given by

$$\overline{Q_{eng}}(z) = \frac{1}{T}\int_0^T \int H_{eng}(x, z, t) w(x, z, t) \mathrm{d}x\mathrm{d}t. \tag{5.8}$$

Time-averaged results for both the free and wall plume are shown in figure 11. We find that for the free plume $\overline{Q_{eng}}/\overline{Q} = 0.072 \pm 0.01$ and $\overline{Q_{out}}/\overline{Q} = 0.060 \pm 0.007$ and for the wall plume $\overline{Q_{eng}}/\overline{Q} = 0.063 \pm 0.01$ and $\overline{Q_{out}}/\overline{Q} = 0.11 \pm 0.01$. Again we see that more ambient fluid is engulfed by the meandering of the free plume compared with the wall plume.

5.4. *Turbulent fluxes*

Measurements of velocity and buoyancy fluctuations and turbulent transport for the free and wall plume experiments are shown in figures 12 and 13, respectively, where the subscript *rms* denotes the root mean square of the data. Our results for the free plume turbulent transport of buoyancy closely follow those of Ramaprian & Chandrasekhara (1989), and the turbulent buoyancy fluctuations are consistent with those of Sangras *et al.* (1998). For both plumes we note that the turbulent buoyancy fluxes are at most about 5% of the mean vertical buoyancy flux. The turbulent fluctuations for the wall plume agree well with those of Sangras *et al.* (1999) and Sangras *et al.* (2000). To our knowledge, turbulent transport quantities for a wall plume in a self-similar region have not been calculated in previous studies, except within a developing region by Lai & Faeth (1987). It is clear that their flow is not self-similar where their measurements are taken, and both this present study and Sangras *et al.* (2000) find significantly larger velocity turbulent fluctuations compared to Lai & Faeth (1987) and, therefore, further comparison between our results is not insightful.

Significantly larger maximum values for the normalised Reynolds stress 0.30 are found in the free plume compared with 0.22 in the wall plume. The maximum values for the

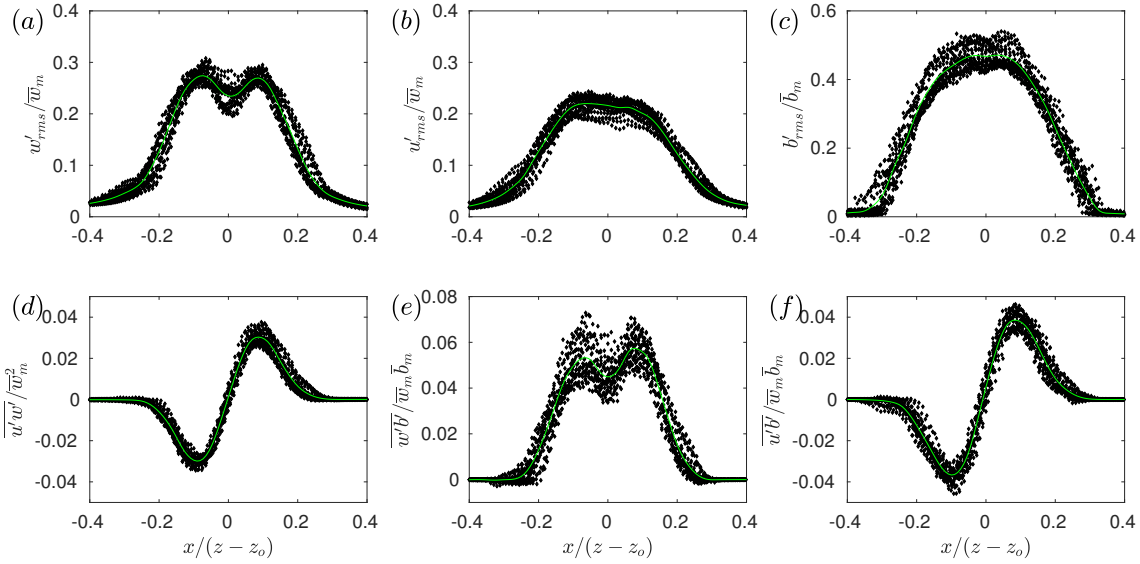

FIGURE 12. Time-averaged scaled free plume turbulent fluctuations of (*a*) vertical velocity, (*b*) horizontal velocity and (*c*) buoyancy and (*d*) Reynolds stress, (*e*) vertical and (*f*) horizontal turbulent buoyancy flux. The green curves are the averages of the data.

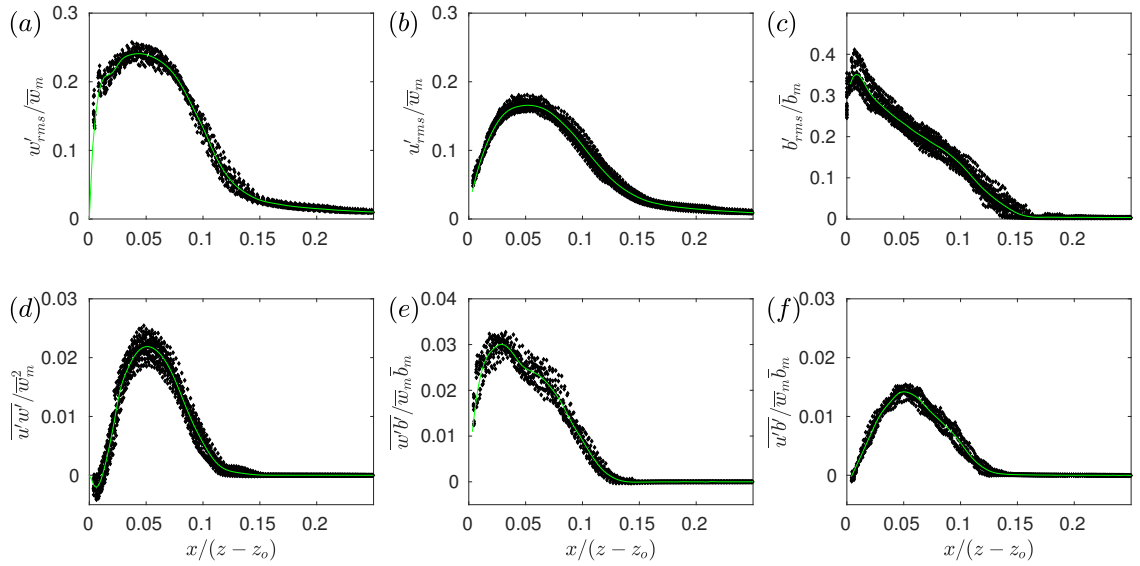

FIGURE 13. Time-averaged scaled wall plume turbulent fluctuations of (*a*) vertical velocity, (*b*) horizontal velocity and (*c*) buoyancy and (*d*) Reynolds stress, (*e*) vertical and (*f*) horizontal turbulent buoyancy flux. The green curves are the averages of the data.

normalised turbulent horizontal and vertical fluxes are also significantly higher in the free plume being, in both cases, approximately double those of the wall plume. The kink observed in the vertical buoyancy flux, figure 13 (e), at about $x/(z-z_o) = 0.08$ appears to be real, as opposed to resulting from scattered data, since it is reflected in the turbulent buoyancy fluctuations, also observed by Sangras *et al.* (1999).

5.5. *Discussion*

Our results may be set in context with the original observation of Ellison & Turner (1959) that the reduced entrainment in the wall plume is due to the suppression of the meandering of the plume. We find that the meandering of the free plume creates coherent structures at the size of the total plume width that frequently overturn and engulf ambient fluid. This in turn stretches the interface leading to an increase in the total length of the TNTI. This suggests that the entrainment process may be viewed as a multi-scale continuous process, where ultimately, at the smallest scales, fluid is nibbled across the TNTI and then irreversibly mixed. The observation that the total TNTI length of the free plume is 2.5 times that of the wall plume is then reflected well in the observation that free plume entrains approximately 2.4 times that of the wall plume. We find that the relative vertical transport of the engulfed fluid, $\overline{Q_{eng}}/\overline{Q}$, of the free plume is approximately 14% greater than the wall plume (see figure 11). However, the relative vertical transport of the ambient fluid outside the TNTI envelope of the wall plume, $\overline{Q_{out}}/\overline{Q}$, is approximately double that of the free plume. Further, $\overline{Q_{out}}$ and $\overline{Q_{eng}}$ are similar in the free plume whereas $\overline{Q_{out}}$ is almost double $\overline{Q_{eng}}$ in the wall plume. This suggests that the wall plume is relatively inefficient at engulfing the outer ambient fluid, whereas the free plume is able to maintain a balance between the vertical transport of ambient and engulfed fluid.

6. Results in a plume coordinate system

6.1. *Plume coordinate system definition*

Following the analysis of Burridge *et al.* (2017) of an axisymmetric plume, we examine the two flows in a coordinate system which follows the plumes as they fluctuate in width. For the free plume the coordinate system, $x_p(z,t)$, is defined by the left, $x_p(z,t) = -X_p(z,t) = E_L(z,t)$, and right, $x_p(z,t) = X_p(z,t) = E_R(z,t)$, TNTI where $x_p(z,t) = 0$ is the instantaneous mid point between the two edges. The coordinate system for the wall plume is similarly defined, however $x_p(z,t) = 0$ remains fixed at the wall, with $x_p(z,t) = X_p(z,t)$ defined at the outer TNTI. Evidently from figure 14 multiple TNTIs can exist for a given height, so the outermost TNTIs are taken as the respective left and right TNTI. Further, prior to the coordinate transformation, the data are conditioned on whether plume fluid is present within the outer plume envelope using the step function H_{eng}, therefore ensuring that all statistics within the region $|x_p| < X_p$ are those within plume fluid. The time-averaged vertical velocity data in plume coordinates is then defined by

$$\overline{w_p} = \overline{w(x_p,z)} = \frac{1}{T_c}\int_0^T w(x_p,z,t)\,[1 - H_{eng}(x_p,z,t)]\,\mathrm{d}t, \tag{6.1}$$

for the total recording time T and the conditional time T_c and the horizontal velocity $\overline{u_p}$ and buoyancy $\overline{b_p}$ are equivalently defined. The turbulent fluctuations and fluxes of the quantities in the plume coordinates are defined with respect to the time-averaged

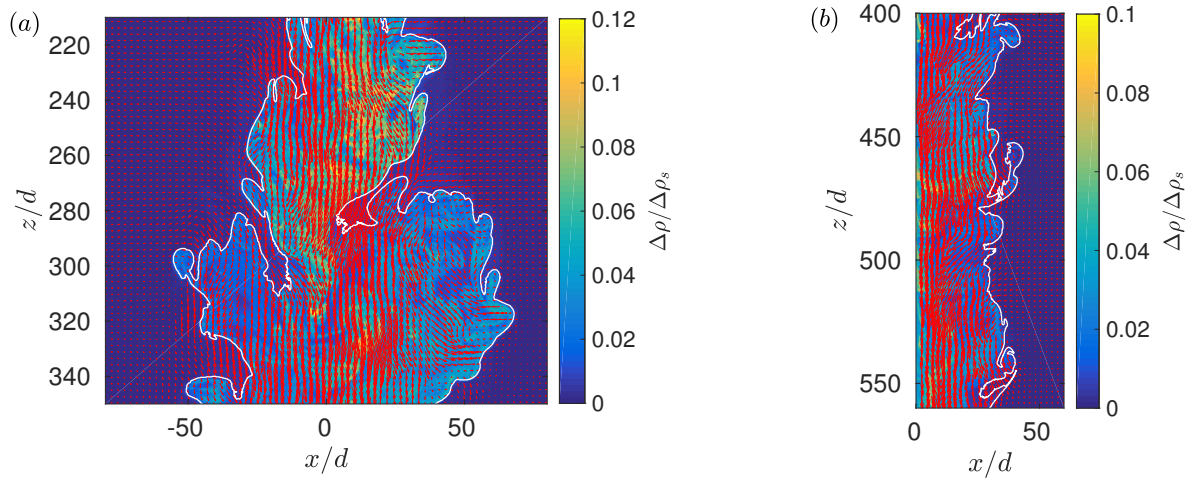

FIGURE 14. Instantaneous buoyancy field overlayed with velocity field, red arrows, from a (*a*) free and (*b*) wall plume experiment. The outer TNTI is highlighted in white.

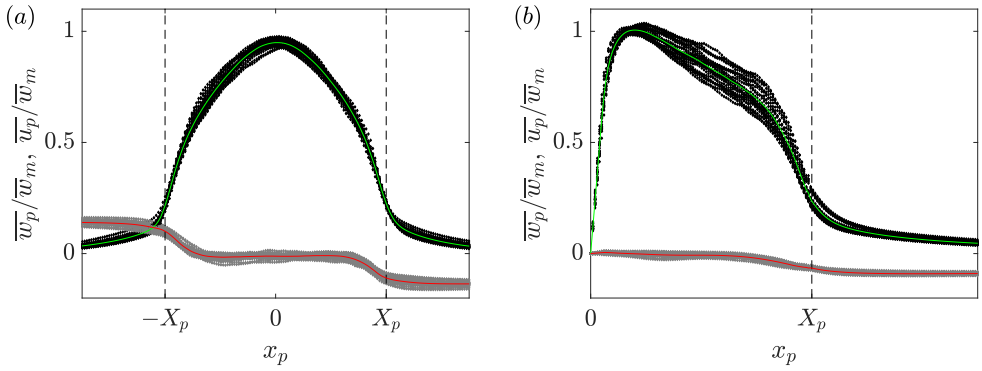

FIGURE 15. The time-averaged vertical velocities, black, and horizontal velocities, grey, in plume coordinates for the (a) free plume and (b) wall plume. The black dashed lines at $x_p = \{-X_p, X_p\}$ highlights the position of the outer TNTI. The green curves are the averages of the data.

quantities in plume coordinates, e.g. for the turbulent vertical velocity fluctuations,

$$w'_{p,rms} = \left(\frac{1}{T_c} \int_0^T \left(w(x_p, z, t) \left[1 - H_{eng}(x_p, z, t) \right] - \overline{w_p} \right)^2 \mathrm{d}t \right)^{1/2}, \tag{6.2}$$

and equivalently for the horizontal velocity $u'_{p,rms}$ and buoyancy fluctuations $b'_{p,rms}$.

6.2. *Velocity and buoyancy in plume coordinates*

The conditionally averaged velocity and buoyancy data in plume coordinates across all experiments are shown in figures 15 and 16, respectively. Data are taken from ten heights spanning the examined region for each experiment.

The average data for both set of experiments collapse onto a single curve showing that the velocities and buoyancy are self-similar when viewed in plume coordinates. The vertical velocities and buoyancy have been scaled by the maximum, time-averaged, vertical

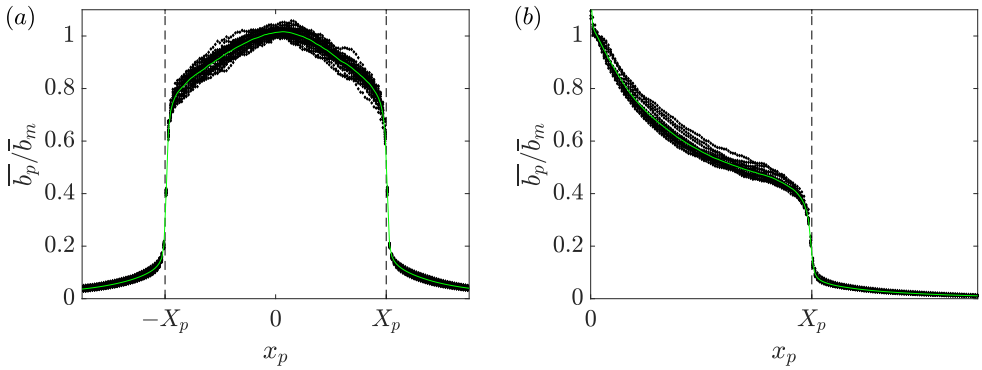

FIGURE 16. The time-averaged buoyancy in plume coordinates for the (a) free plume and (b) wall plume. The black dashed lines at $x_p = \{-X_p, X_p\}$ highlights the position of the outer TNTI. The green curves are the averages of the data.

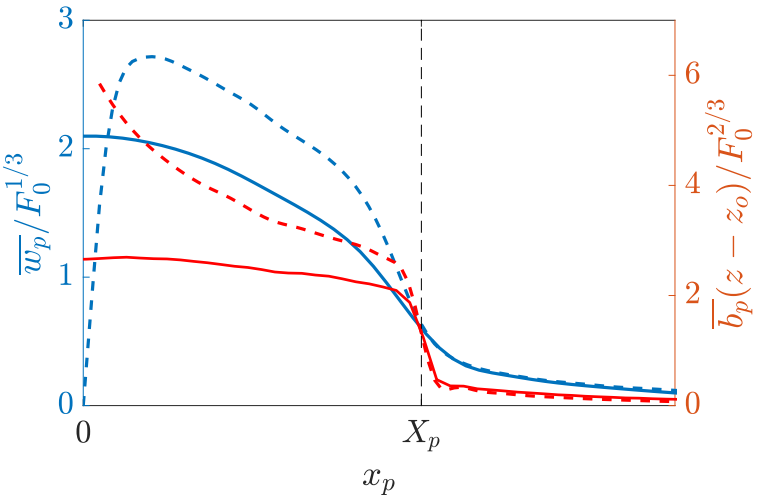

FIGURE 17. Average profiles of the time-averaged free (solid) and wall plume (dashed) vertical velocities (blue, left) and buoyancy (red, right) in plume coordinates. Only half the region of the free plume is shown, $x_p \geq 0$ to aid comparison with the wall plume. The vertical velocities have been scaled using the buoyancy flux and the buoyancy has been scaled using the buoyancy flux and distance from the virtual origin.

velocity and buoyancy measured in Eulerian coordinates, respectively. The maximum time-averaged buoyancy, in the plume coordinate system, is greater than that in the Eulerian coordinate system, for both the free and wall plume. This is to be expected, since the contribution of the ambient fluid in the calculation of the mean buoyancy is omitted in the plume coordinate system. However, it is surprising to note that the maximum vertical velocity of the free plume in the plume coordinate system is lower than that in the Eulerian coordinate system. This may be due to the meandering of the plume and is not observed in the wall plume, where as one would expect from considering the additional buoyancy, the maximum velocity is greater in the plume coordinate system.

The average vertical velocities at the plume edge (dashed vertical lines at $\{-X_p, X_p\}$) for the free plume are significant, on average 23% of the centreline velocities. This is almost identical to the behaviour of an axisymmetric plume observed by Burridge *et al.* (2017) where the vertical velocities at the outer TNTI of the plume were also found to be about 20% of the centreline velocities. This behaviour is similarly observed in the wall plume where the vertical velocities at the outer TNTI are on average 25% of the maximum vertical velocity.

The buoyancy profile in plume coordinates of the free plume in figure 16 (*a*) shows that there is a jump in buoyancy at the interface of about 75% of the centreline buoyancy. This is surprisingly large and significantly greater than the jump in passive scalar at the interface observed in an axisymmetric jet by Westerweel *et al.* (2002). The jump in buoyancy at the interface for the wall plume figure 16 (*b*) is significantly lower than the free plume at about 40% of the maximum buoyancy. The free plume buoyancy profile broadly exhibits a constant gradient, of opposite sign, either side of the centreline. This is in contrast to the wall plume, where the gradient is rapidly increasing in magnitude from the interface towards the wall. The profiles show that there exists buoyancy outside the outer TNTI of the plume. These values of b are due to background light and noise associated with the LIF images, however, the sharp jump in buoyancy at $x_p = \pm X_p$ validates the correct use of the threshold used to determine the TNTI.

To highlight the differences between the two flows, figure 17 shows the average of all the data of the time-averaged vertical velocities and buoyancy in plume coordinates of the free and wall plume, where the vertical velocities have been scaled using the buoyancy flux and the buoyancy has been scaled using the buoyancy flux and virtual distance from the source. Only the region $x_p \geq 0$ is shown for the free plume. This shows that, for a given buoyancy flux, the vertical velocity profiles of the wall plume and free plume outside the plume are almost indistinguishable, in particular the vertical velocities at the outer TNTI, $x_p = X_p$, are identical. Similarly, for a given buoyancy flux and distance from the virtual source, the buoyancy at the outer TNTI of the free and wall plumes are almost identical. The vertical velocity of the wall plume increases, in the negative x direction, away from the TNTI more rapidly than the free plume. This is expected given the larger buoyancy in the wall plume. In the adjustment region $0.8 < x_p/X_p < 1$ the buoyancy rapidly increases for both the free and wall plume. However, away from this adjustment region within the plume, $x_p/X_p < 0.8$, the buoyancy of the free plume changes at most by 9% of the mean buoyancy within that region, whereas the wall plume changes by 52% of the mean buoyancy within that region. This shows that the free plume is more well-mixed than the wall plume. This implies that there is a more equal distribution of buoyancy force across the plume, which results in a more top-hat vertical velocity in plume coordinates, which can be seen in figure 17.

6.3. *Turbulent fluctuations and fluxes in plume coordinates*

The vertical velocity fluctuations in the plume coordinate are shown in figures 18 (*a*) and 19 (*a*) for the free and wall plume, respectively. The profile of the free plume broadly mirrors that observed in Eulerian space, with bi-modal peaks at 30% of the maximum Eulerian vertical velocity. This is larger than the bi-modal peaks observed in Eulerian space, a result similarly observed in axisymmetric plumes (Burridge *et al.* 2017), where it was suggested that the meandering of the plume masks the scale of the turbulent velocity fluctuations. The profile of the vertical velocity fluctuations in the wall plume is quite different from Eulerian space. Three distinct peaks are observed: one very close to the wall, a second peak within the middle of the plume region and a third peak almost exactly at the outer TNTI of the plume. The maximum peak is on average 25% of the

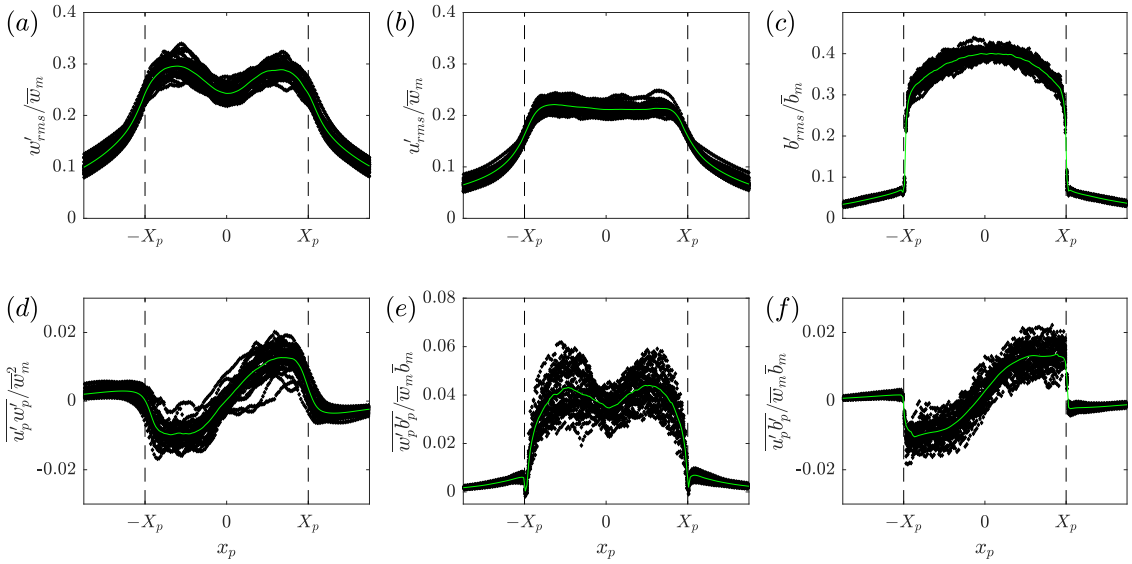

FIGURE 18. Time-averaged scaled free plume turbulent fluctuations in plume coordinates of (*a*) vertical velocity, (*b*) horizontal velocity and (*c*) buoyancy and (*d*) Reynolds stress, (*e*) vertical and (*f*) horizontal turbulent buoyancy flux. The green curves are the averages of the data.

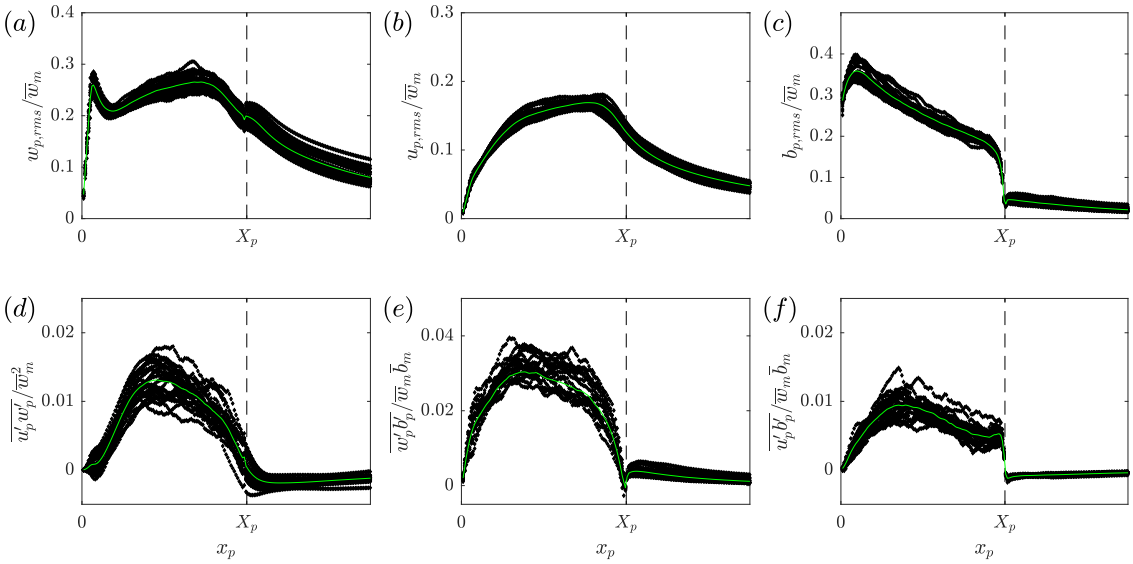

FIGURE 19. Time-averaged scaled wall plume turbulent fluctuations in plume coordinates of (*a*) vertical velocity, (*b*) horizontal velocity and (*c*) buoyancy and (*d*) Reynolds stress, (*e*) vertical and (*f*) horizontal turbulent buoyancy flux. The green curves are the averages of the data.

maximum Eulerian vertical velocity. This peak value is almost identical to that observed in Eulerian space. The reduced meandering of the wall plume may explain the reduced effect of the increase in magnitude of turbulent velocity fluctuations seen in the free and axisymmetric plume.

The buoyancy fluctuations of the free and the wall plume in figures 18 (*c*) and 19 (*c*), respectively, are very different to the Eulerian statistics. This is expected, since there must be ambient fluid, i.e $b = 0$ except for any additional noise associated with the experiment, beyond the outer TNTI and therefore a jump is observed at $x_p = \pm X_p$ in both flows. The maximum buoyancy fluctuations in both the free and wall plume are less than those in the Eulerian statistics. This results from the condition that the ambient fluid is omitted in the calculation of the statistic. A larger discrepancy between the plume and Eulerian coordinate system is observed in the free plume. This is presumably because of the increased meandering and engulfment of the free plume.

The Reynolds stress profiles of the free and the wall plume in plume coordinates are shown in figures 18 (*d*) and 19 (*d*), respectively. An interesting feature, which is also observed in axisymmetric plumes (Burridge *et al.* 2017), is the change of sign across the region of the plume edge. For comparison consider only the region $x_p \geq 0$ of the free plume, but note that results are equivalent although of opposite sign for $x_p \leq 0$. In this case, as with the wall plume in the region away from the wall, $\overline{u_p' w_p'}$ is positive within the plume, however it rapidly becomes negative within the ambient fluid. This is contrast to the Eulerian statistic, where $\overline{u'w'}$ is positive and gradually tends to zero in the positive x direction, presumably because the Reynolds stress is larger in magnitude within the plume region and, as with the velocity fluctuations, the meandering of the plume masks the ambient flow statistics. The negative Reynolds stress outside the plume may be explained from considering the entrainment process. The negative correlation $\overline{u_p' w_p'} < 0$ suggests either transport of streamwise momentum inwards or transport of negative streamwise momentum outwards. The former is consistent with the observation that $w'_{p,rms} > 0$ (figures 18 (*a*) and 19 (*a*)) and is associated with entrainment since it is necessary for transport of fluid from the non-turbulent ambient into the turbulent plume region, and is described by Odier *et al.* (2012) for a gravity current. The latter would imply detrainment of slower moving plume fluid which is not observed. The peak Reynolds stresses in plume coordinates, in both cases, are lower in magnitude than the Eulerian Reynolds stresses. This is also observed in axisymmetric plumes and it is not clear why this should occur.

The turbulent vertical buoyancy flux in plume coordinates of the free plume (figure 18 (*e*)) shows a bi-modal peak with maximum values on average of 30% larger than those observed in Eulerian coordinates. The omission of ambient data presumably has a similar effect on reducing $\overline{w_p' b_p'}$. The turbulent buoyancy flux in plume coordinates of the wall plume, 19 (e) looks quite different from the Eulerian statistic. The profile is more similar to a top-hat profile, and the kink seen in Eulerian coordinates is not observed. This, therefore, suggests the kink is a consequence of the combined ambient and plume statistics in the Eulerian coordinate system, especially since it is located close to the mean position of the plume edge. It is not clear, then, why this property should not also be observed in the free plume. Maximum values of $\overline{w_p' b_p'}$ and $\overline{w'b'}$ are broadly the same.

It is interesting to note the differences in the turbulent horizontal buoyancy flux $\overline{u_p' b_p'}$ between the free and wall plumes in plume coordinates, figures 18 (*f*) and 19 (*f*), respectively. Again considering only the region $x_p \geq 0$ of the free plume, the gradient of $\overline{u_p' b_p'}$ is mostly positive in the free plume whereas in the wall plume it is mostly negative.

Further, peak values are observed very close to plume edge in free plume whereas in the wall plume they are observed at about $x_p/X_p = 0.4$.

We also emphasise that the observations of §5.2 are consistent with the statistics of the plume in plume coordinates. It was shown that, on average, the local entrainment velocity at the viscous scale was larger in the wall plume than the free plume. The local entrainment velocity is driven by the momentum jump at the TNTI (Westerweel *et al.* 2009), therefore larger local entrainment flux is consistent with the observation of larger conditional Reynolds stress and buoyancy in the wall plume. Given that, for a given buoyancy flux, $\overline{w}_{m,w}/\overline{w}_{m,f} = 1.29$, figures 18 (*d*) and 19 (*d*) suggest that for a given buoyancy flux the peak Reynolds stress in the wall plume is larger than the peak Reynolds stress in the wall plume by a factor of 1.8.

7. Conclusions

Simultaneous velocity and buoyancy field measurements of a free and wall plume provided direct measurements of the top-hat entrainment coefficients. We found that the entrainment coefficient of the free plume $\alpha_f = 0.14$ is slightly less than double that of the wall plume $\alpha_w = 0.08$. However, it was shown that, for a given buoyancy flux, this corresponds to the free plume physically entraining more than double per unit height than the wall plume, as expressed in terms of the rate of increase in plume volume flux with height $\mathrm{d}Q_f/\mathrm{d}z = 2.4\mathrm{d}Q_w/\mathrm{d}z$.

To account for this difference in entrainment the statistics of the TNTI were calculated. We provided evidence of the free plume meandering and, in particular, we showed that there is a significant probability, about 15%, of ambient fluid outside the plume TNTI existing at the centreline, suggesting coherent lateral/sideways meandering of the plume centreline. This is in contrast to an axisymmetric plume where no coherence between the left and right TNTI of the plume were observed (Burridge *et al.* 2017). Through this meandering it was shown that the TNTI is stretched and on average the total length of TNTI of the free plume is longer than the wall plume by a factor of about 2.5, measured at a resolution close to the Kolmogorov length scale.

The data were conditioned on whether plume fluid was present or absent which allowed the vertical transport of the ambient and engulfed fluid to be calculated, separately. It was found that the proportion of vertical transport of the engulfed ambient fluid of the free plume was larger than that of the wall plume. This suggests increased engulfment in the free plume which, as shown in Burridge *et al.* (2017) for an axisymmetric plume, is a dominant mechanism in the entrainment process.

The turbulent velocity and buoyancy fluctuations were measured and the resulting turbulent fluxes and Reynolds stresses were calculated. Larger peak values were observed across all the fluctuations and turbulent fluxes in the free plume, resulting from larger turbulence production in the free plume. However, by relating the global entrainment flux to the local entrainment at the viscous scale of the TNTI, it was shown that the local entrainment velocity is on average greater in the wall plume than the free plume. This is consistent with the conditional plume statistics, where larger Reynolds stresses and buoyancy were observed in the wall plume in plume coordinates, suggesting a larger vertical momentum jump at the edge of the plume driving the entrainment flux across the TNTI. This increased entrainment at the small scales somewhat compensates for the smaller length of the TNTI compared with the free plume so that the entrainment constant for the wall plume is slightly larger than half that of the free plume.

While the presence of the wall is the only fundamental difference between the free and wall plume, the effect of the wall could be viewed as two separate processes, namely the

no-slip condition and the impermeability condition. We show that the wall shear stress is non-negligible and this results in a reduction of momentum of the wall plume, which could otherwise be used in the turbulent production contributing to entrainment. Alternatively, the impermeability condition prevents the wall plume meandering which both the reduces the large scale engulfment process and the stretching of the TNTI leading to a shorter total TNTI. It is difficult to separate these two processes and provide an answer to the which is the dominant effect in the reduction of entrainment in the wall plume. It would be interesting to resolve this issue numerically by comparing a simulation of a wall plume with a no-slip and a free-slip condition.

Acknowledgements

We are grateful to the skilled technical staff of the G. K. Batchelor Laboratory for the manufacture of the apparatus and the illumination system. We also wish to acknowledge the contribution of Prof. Stuart Dalziel to the data capture and processing. The work has received financial support from the UK Engineering and Physical Sciences Research through an iCASE award with Arup and also through the Programme Grant EP/K034529/1 'Mathematical Underpinnings of Stratified Turbulence' (MUST), and from the European Research Council through the Horizon 2020 research and innovation programme agreement number 742480 'Stratified turbulence and mixing processes' (STAMP).

REFERENCES

Burridge, H. C., Parker, D. A., Kruger, E. S., Partridge, J. L. & Linden, P. F. 2017 Conditional sampling of a high pclet number turbulent plume and the implications for entrainment. *Journal of Fluid Mechanics* **823**, 2656.

Ellison, T. H. & Turner, J. S. 1959 Turbulent entrainment in stratified flows. *Journal of Fluid Mechanics* **6**, 423–448.

Fischer, H.B., List, J.E., Imberger, J., Koh, C.R. & Brooks, N.H. 1979 *Mixing in Inland and Coastal Waters*. Academic Press.

Grella, J. J. & Faeth, G. M. 1975 Measurements in a two-dimensional thermal plume along a vertical adiabatic wall. *Journal of Fluid Mechanics* **71**, 701–710.

Kotsovinos, N 1975 Study of the entrainment and turbulence in a plane buoyancy jet. *California Institute of Technology , Pasadena, CA* .

Lai, M.-C. & Faeth, G.M. 1987 Turbulent structure of vertical adiabatic wall plumes. *Journal of Heat Transfer* **109** (3), 663–670.

Lee, S. L. & Emmons, H. W. 1961 A study of natural convection above a line fire. *Journal of Fluid Mechanics* **11**, 353–368.

Meneveau, Charles & Sreenivasan, K. R. 1990 Interface dimension in intermittent turbulence. *Phys. Rev. A* **41**, 2246–2248.

Mistry, Dhiren, Dawson, James R. & Kerstein, Alan R. 2018 The multi-scale geometry of the near field in an axisymmetric jet. *Journal of Fluid Mechanics* **838**, 501515.

Mistry, Dhiren, Philip, Jimmy, Dawson, James R. & Marusic, Ivan 2016 Entrainment at multi-scales across the turbulent/non-turbulent interface in an axisymmetric jet. *Journal of Fluid Mechanics* **802**, 690725.

Morton, B. R., Taylor, G. I. & Turner, J. S. 1956 Turbulent gravitational convection from maintained and instantaneous sources. *Proc. R. Soc. Lond.* **234**, 1–24.

Odier, P., Chen, J. & Ecke, R.E. 2012 Understanding and modeling turbulent fluxes and entrainment in a gravity current. *Physica D: Nonlinear Phenomena* **241** (3), 260268, special Issue on Small Scale Turbulence.

Paillat, S. & Kaminski, E. 2014 Entrainment in plane turbulent pure plumes. *Journal of Fluid Mechanics* **755**, R2.

Prasad, R. R. & Sreenivasan, K. R. 1989 Scalar interfaces in digital images of turbulent flows. *Experiments in Fluids* **7** (4), 259264.

Ramaprian, B. R. & Chandrasekhara, M. S. 1989 Measurements in Vertical Plane Turbulent Plumes. *Journal of Fluids Engineering* **111**, 69–77.

van Reeuwijk, M, Salizzoni, P, Hunt, GR & Craske, J 2016 Turbulent transport and entrainment in jets and plumes: A dns study. *PHYSICAL REVIEW FLUIDS* **1**.

Rouse, H, YIH, C. S. & Humphreys, H. W. 1952 Gravitational Convection from a Boundary Source. *Tellus* **4** (3), 201210.

Sangras, R., Dai, Z. & Faeth, G.M. 1999 Mixture Fraction Statistics of Plane Self-Preserving Buoyant Turbulent Adiabatic Wall Plumes. *Journal of Heat Transfer* **121** (4), 837843, 10.1115/1.2826073.

Sangras, R., Dai, Z. & Faeth, G.M. 2000 Velocity statistics of plane self-preserving buoyant turbulent adiabatic wall plumes. *Journal of Heat Transfer* **122** (4), 693–700.

Sangras, R., Dai, Z. & Faeth, G. M. 1998 Mixing structure of a plane self-preserving buoyant turbulent plumes. *Journal of Heat Transfer* **120**, 1033–1041.

de Silva, Charitha M., Philip, Jimmy, Chauhan, Kapil, Meneveau, Charles & Marusic, Ivan 2013 Multiscale geometry and scaling of the turbulent-nonturbulent interface in high reynolds number boundary layers. *Phys. Rev. Lett.* **111**, 044501.

Turner, J. S. 1973 Buoyancy effects in fluids .

Westerweel, J., Fukushima, C., Pedersen, J. M. & Hunt, J. C. R. 2005 Mechanics of the turbulent-nonturbulent interface of a jet. *Phys. Rev. Lett.* **95**, 174501.

Westerweel, J., Fukushima, C., Pedersen, J. M. & Hunt, J. C. R. 2009 Momentum and scalar transport at the turbulent/non-turbulent interface of a jet. *Journal of Fluid Mechanics* **631**, 199230.

Westerweel, J., Hofmann, T., Fukushima, C. & Hunt, J. 2002 The turbulent/non-turbulent interface at the outer boundary of a self-similar turbulent jet. *Experiments in Fluids* **33** (6), 873878.

Yuana, Li-Ming & Cox, G. 1996 An experimental study of some line fires. *Fire Safety Journal* **27** (2), 123139.